Combined experimental and theoretical investigation of optical, structural, and electronic properties of $CH_3NH_3SnX_3$ thin films (X=Cl,Br)

Fabio Chiarella, Andrea Zappettini, and Francesca Licci
IMEM-CNR, Area delle Scienze 37/A, I-43100 Parma, Italy

Ivo Borriello, Giovanni Cantele, Domenico Ninno, Antonio Cassinese, and Ruggero Vaglio
Coherentia CNR-INFM and Dipartimento di Scienze Fisiche, Università of Napoli "Federico II," Via Cinthia, I-80126, Napoli, Italy

(Received 12 January 2007; revised manuscript received 2 October 2007; published 25 January 2008)

Well-oriented thin films of methyl-ammonium trihalogenostannates $CH_3NH_3SnX_3$ compounds (X=Cl,Br) are grown by the single source thermal ablation technique. Optical absorption and structural analysis of $CH_3NH_3SnX_3$ thin films are combined with *ab initio* calculations in order to clarify their electronic properties and the role of the organic cation. The structural calculations reproduce well the measured lattice parameters, and optical measurements reveal a direct gap absorption onset for both compounds, in agreement with the calculated band structures. It turns out from projected density of states analysis that the valence and conduction bands take negligible contribution from the methylammonium. It is inferred that the band gap mainly depends on the ionicity and size of the inorganic cage SnX_3.

DOI: 10.1103/PhysRevB.77.045129 PACS number(s): 78.66.Li, 31.15.E−, 81.15.Ef

I. INTRODUCTION

The ABX_3, A_2BX_4, and ABX_4 compounds, where A is an amine (R-NH_3^+) or diamine (NH_3^+-R-NH_3^+) cation, R an organic radical, B a divalent metal, and X a halide, belong to the organic-inorganic perovskite hybrid class.[1] The hybrid A_2BX_4 and ABX_4 compounds are formed by inorganic layers referred to as "perovskite sheets" because they have great analogy with the inorganic layered perovskites (as the Ruddlesden-Popper series[2]) and they are conceptually derivable from the three-dimensional ABX_3 perovskite structure by taking a one-layer-thick cut along a crystallographic direction.[1] These hybrid perovskite materials, composed of organic and inorganic units, have been shown to have interesting physical properties and to be suitable for technological applications.[3] Relevant results such as metal-insulator transition,[4] two-dimensional magnetism,[5] excitonic light emission over the full range of visible wavelengths,[6] and organic-like mobility performance[7] have been reported in literature. Moreover, simple synthesis and cheap thin film deposition processes can be achieved[8] due to their self-assembling character. In all these activities, the possibility of tuning the physical properties by changing a single component and/or exploring the dimensionality of the inorganic cage has been demonstrated. In this framework, the comprehension of the correlations between structure, chemical composition, and properties through first-principles calculations can give the possibility of designing new functional structures, with desired physical properties.

The $CH_3NH_3BX_3$ compounds are a subclass of the ABX_3 family, with cubic structures where the organic component is included in the extended three-dimensional inorganic cage. The negative charge is typically localized on the halide atoms and the $CH_3NH_3^+$ cation occupies the center of the cubic cell. In these structures, the divalent metal (B) is in octahedral coordination with halogen atoms forming classical perovskitic octahedra.

At high temperature, $CH_3NH_3^+$ is free to rotate because the potential barriers between the different stable configurations are smaller than the thermal energy and so all these compounds own a high temperature cubic phase. This is confirmed by the experimental[9] findings demonstrating, on the basis of nuclear magnetic resonance and nuclear quadrupolar resonance, that $CH_3NH_3^+$ cations undergo rapid isotropic reorientation at room temperature in the $CH_3NH_3PbX_3$ (X=Cl,Br,I) lead compounds. A similar behavior is found[10,11] in isostructural compounds such as tin(II) halide $CH_3NH_3SnX_3$ compounds.

Previous studies[10–13] on $CH_3NH_3SnX_3$ pellets showed that, in this class of compounds, transport properties seem to evolve from metallicity to semiconductivity along the series I→Br→Cl. In this work, absorption analysis, room-temperature resistivity, and x-ray structural analysis on $CH_3NH_3SnX_3$ thin films (with X=Cl,Br) are combined with *ab initio* calculations in order to understand their electronic properties and the role of the organic cation into the band structures.

The paper is organized as follows. Section II describes the experimental (Sec. II A) and theoretical (Sec. II B) methods. The experimental results are analyzed in Sec. III. In Sec. IV, we analyze the computational results and compare them to the experiment. Finally, in Sec. V, some conclusions are drawn.

II. METHODOLOGY

A. Experimental setup

Films of $CH_3NH_3SnX_3$ compounds (X=Cl,Br) are grown at room temperature on glass and quartz substrates by single source thermal ablation technique[8] from mechanically mixed reagents (more details are reported elsewhere[14]). $CH_3NH_3SnBr_3$ films appear red-orange colored and iridescent while $CH_3NH_3SnCl_3$ films appear whitish transparent.

Film homogeneity and morphology are tested by scanning electron microscopy analysis and standard profilometry is used to measure their thickness and roughness. Typical film

thickness ranges between 500 nm and 1 μm, showing a 100 nm averaged grain size and a roughness of about 5% of the thickness. The structural properties of the films and powders have been characterized using D-500 Siemens Cu $K\alpha$ x-ray diffractometer.

The optical absorption of films deposited on quartz were recorded in the energy range of 1.1–6.5 eV using a JASCO V-530 dual beam scanning spectrophotometer. The resistance of the films were measured by a standard two-probe technique.[14] The electrical gold contacts (9 mm wide and 0.1 mm distant) were deposited by evaporating metallic gold in the presence of appropriate stencil-steel masks.

B. Theoretical approach

To shed light on the nature of the observed optical transitions and on the role played by the cation in the perovskitic cage, we have performed *ab initio* calculations in the framework of density functional theory (DFT), as implemented in the QUANTUM-ESPRESSO package.[15] The calculations have been performed using a plane-wave basis set for the expansion of the single-particle Kohn-Sham wave functions and pseudopotentials to describe the computationally expensive electron-ion interaction.

Vanderbilt-type ultrasoft pseudopotentials[16] have been used to represent all atoms except for bromine (Br), for which a Troullier-Martin[17] norm-conserving pseudopotential has been selected. The generalized gradient approximation (GGA) with the Perdew and Wang[18] parametrization was employed for the evaluation of the exchange-correlation energy. The electronic wave functions have been expanded using plane waves corresponding to energies up to 30 Ry, while a 180 Ry cutoff energy has been used to represent the total charge density. A $4\times4\times4$ Monkhorst-Pack grid[19] has been chosen for sampling the Brillouin zone. Full relaxation of the atomic positions within the unit cell is allowed following the Broyden-Fletcher-Goldfarb-Shanno algorithm. For all the considered structures, the theoretical optimal lattice parameters have been calculated.

To give a better estimation of the band gap, we have calculated GW many-body corrections[20] to the DFT-GGA energy gaps at the optimized geometries using the ABINIT code.[21] In this case, Troullier-Martin[17] norm-conserving pseudopotentials have been used to represent the atomic nuclei with the Perdew-Burke-Ernzerhof parametrization[22] for the exchange-correlation energy with a plane-wave basis set cutoff energy of 100 Ry.

III. EXPERIMENTAL RESULTS

Room-temperature diffraction analysis of polycrystalline powders of the $CH_3NH_3SnCl_3$ compound [Fig. 1(c)] has revealed that the powders do not result in a cubic phase but are distorted in a monoclinic or triclinic phase. As reported by Yamada *et al.*,[23] these two distorted cubic structures show only minor differences. The differences of the cell parameters (α and γ angles[24] change from 90° to 90.37° and 90.05°, respectively) do not seem appreciable by our analysis; however, monoclinic refinement was carried out.

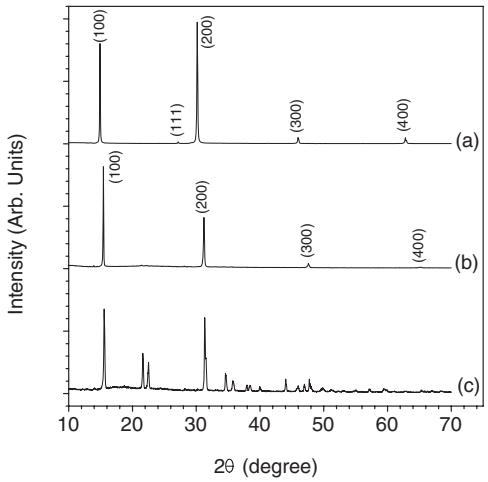

FIG. 1. X-ray diffraction patterns of (a) $CH_3NH_3SnBr_3$ and (b) $CH_3NH_3SnCl_3$ films. The diffraction pattern of the powders of $CH_3NH_3SnCl_3$ compound are labeled as (c).

From the analysis of the diffraction patterns of the films of both compounds reported in Figs. 1(a) and 1(b), the films result to be single phased. The $CH_3NH_3SnBr_3$ diffraction pattern is compatible with a cubic perovskite structure.[13,14] The presence of the (ℓ 0 0) set of reflections in the films of both compounds gives an indication of the good crystallization and the occurrence of a dominant crystallographic orientation. The measured *a*-axis lattice parameters of the films, as well as the lattice parameters of the powders for both compounds, are reported in Table I and compared with the calculated ones (see later).

The film resistivity presents a semiconducting temperature behavior and room-temperature resistivity measurements are summarized in Table II.

Absorbance of 500 nm thick films was measured in air at room temperature. The absorption coefficient α, shown in the inset of Fig. 2, was obtained by including corrections for multiple reflections. It can be seen that the absorption edge rapidly rises to values typical for direct-band-gap crystals ($\alpha\sim10^4-10^5$ cm^{-1}). As such, it can be described[25] by the relation $(\alpha h\nu)^2\propto(h\nu-E_g)$, as shown by the linear slope in Fig. 2. In the case of $CH_3NH_3SnBr_3$, the presence of a bump

TABLE I. Comparison between experimental and theoretically calculated parameters for room-temperature phases of $CH_3NH_3SnX_3$ (X=Cl, Br). Lengths are expressed in Å and angles in degrees.

Parameters	Film	Powder	Calculated
	Monoclinic $CH_3NH_3SnCl_3$		
a	5.73(1)	5.69(1)	5.878
b		8.23(1)	8.381
c		7.94(1)	8.013
β		93.2(1)	96.1
	Cubic $CH_3NH_3SnBr_3$		
a	5.88(1)	5.89(1)	6.001

TABLE II. Measured resistivity (ρ) and absorption gap (E_g) for the $CH_3NH_3SnX_3$ films. Computed band gaps (with and without inclusion of the GW many-body correction) are reported as well.

			Theoretical E_g (eV)	
X	ρ (MΩ cm)	Measured E_g (eV)	DFT-GGA	With GW
Br	0.5 ± 0.1	2.15 ± 0.01	1.04	1.90
Cl	1.4 ± 0.1	3.69 ± 0.05	1.94	3.44

is related to an overlap of multiple direct gap contributions to the absorption. Multiple direct band gaps are evident from the calculated band structure (see later). The fitted band-gap values E_g are reported in Table II.

The obtained gap and resistivity values together with previously reported metallic reflectivity and resistivity[12] observed for $CH_3NH_3SnI_3$ compounds show a decrease upon changing the halogen atoms along the $CH_3NH_3SnX_3$ series Cl→Br→I. This can be correlated with the decrease of the Pauling electronegativity of the halogen atom (X) (3.16, 2.96, 2.66 for Cl, Br, I, respectively), resulting in the reduction of the ionicity of the Sn–X bond. To better understand and explain this empirical consideration, we discuss the results of *ab initio* calculations in the next section.

IV. *AB INITIO* RESULTS

A. Structural properties

$CH_3NH_3SnX_3$ crystals exhibit a cubic perovskite structure in the highest temperature phase, although the methylammonium cation $CH_3NH_3^+$ has, at most, a C_{3v} symmetry. The cations in this phase are dynamically disordered, behaving like spherical ions,[26,27] thus satisfying the $m3m$ site symmetry of the crystal. The disorder is removed through one or more phase transitions characterized by SnX_6 octahedra distortions creating potential wells for the NH_3^+ polar head of the $CH_3NH_3^+$ cation, favoring a spontaneous polarization characterized by an ordered orientation of the cations.

At room temperature, $CH_3NH_3SnBr_3$ and $CH_3NH_3SnCl_3$ compounds exhibit different crystal structures, strictly connected to different dynamics of the cation inside the pseudocubic anion cage. The former is found to have a cubic perovskitic structure (disordered orientation), while the latter exhibits a monoclinic structure (ordered orientation).

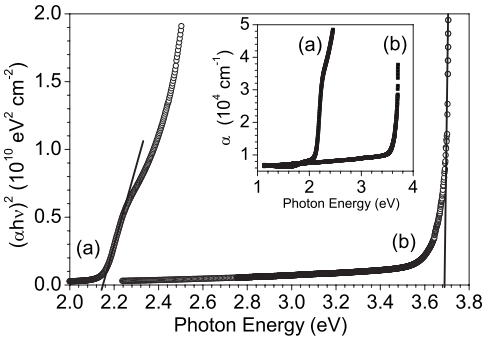

FIG. 2. Fitting to the $(\alpha h\nu)^2 \propto (h\nu - E_g)$ equation, describing direct-band-gap allowed transitions for (a) $CH_3NH_3SnBr_3$ and (b) $CH_3NH_3SnCl_3$ films on quartz. The inset shows the absorption coefficient spectra of the films of both compounds.

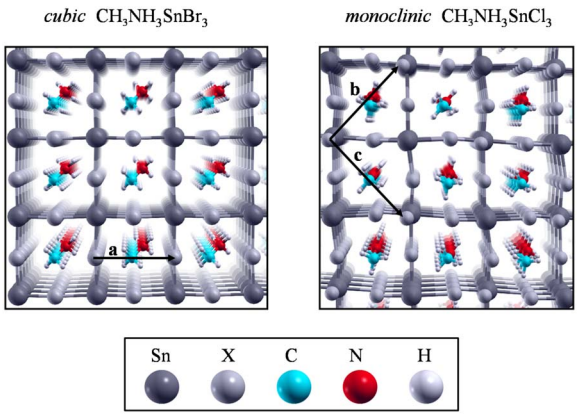

FIG. 3. (Color online) A perspective of $CH_3NH_3SnBr_3$ and $CH_3NH_3SnCl_3$ in the cubic and monoclinic phases, respectively. In both structures, the $CH_3NH_3^+$ cation is enclosed in a pseudocubic SnX_3 (X=Br,Cl) cage. The in-plane lattice constants are also shown.

In Fig. 3, a perspective of both cubic $CH_3NH_3SnBr_3$ and monoclinic $CH_3NH_3SnCl_3$ as obtained by *ab initio* simulation is shown. For both structures, the pseudocubic SnX_3 cage is easily recognizable.

The lattice parameter of the cubic $CH_3NH_3SnBr_3$ obtained from fully relaxed (ions and electrons) geometry is a=6.001 Å, as also reported in Table I, in pretty good agreement with the experimental results. The Sn and Br atoms have been initially placed at the vertex ($m3m$ site symmetry) and at the middle ($4/mmm$ site symmetry) of each side of the cubic cell, respectively, as it is predicted in the case of a perfect perovskitic structure. The $CH_3NH_3^+$ cation has been placed along the cube diagonal, with the middle point of the C-N bond exactly at the center of the cubic cage. The relaxed structure presents a light distortion of the $SnBr_6$ octahedron, strictly connected to the fixed orientation of the cation in the simulation. The Sn-Br bond lengths lie in the range of 2.83–3.17 Å, while the Sn-Br-Sn chain is slightly distorted (with an angle of 176°).

In the case of $CH_3NH_3SnCl_3$, at room temperature, the monoclinic structure is chosen, with a unit cell containing two $CH_3NH_3SnCl_3$ units. In order to obtain the atomic geometry inside the unit cell, we used x-ray diffraction data[23] as a starting point for total energy minimization. *Ab initio* structural parameters of the fully relaxed system are reported in Table I. Theoretical structural results are in good agreement with the experimental data obtained in this work as well as with those reported by Yamada *et al.*[23] Our results on Sn-Cl distances evidence $SnCl_3^-$ anion formation with a trigonal pyramid structure, characterized by a Sn-Cl bond length of about 2.6 Å and a Cl-Sn-Cl angle slightly greater than 90°. Our results reproduce well isolated $SnCl_3^-$ anions experimentally recognized in the distorted octahedral coordination.[23]

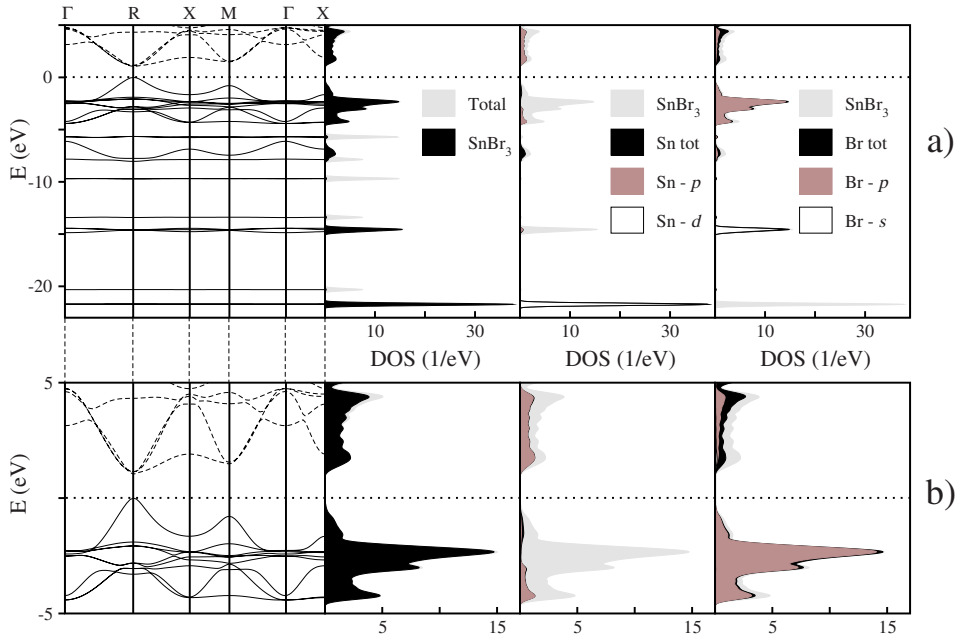

FIG. 4. (Color online) The calculated band structure and the total and the projected density of states for $CH_3NH_3SnBr_3$ in the cubic phase. In panel I, the band structure is shown along the high symmetry directions in the Brillouin zone. In panel II, the total DOS (gray) is represented along with the projection on $SnBr_3$ (black). The visible part of the gray shadow is related to the $CH_3NH_3^+$ cation, in correspondence to flat bands. In panels III and IV, the projected DOS on Sn and Br, respectively, is shown. A closer view of the near band region is shown in (b). Solid (dashed) lines represent full (empty) bands. The dotted line indicates the top of the valence band, set to zero.

B. Electronic properties

The calculated band structures for both compounds along high symmetry directions in the Brillouin zone are shown in Figs. 4 and 5. The energy scale is in eV and the origin of energy was arbitrarily set to be at the valence band maximum. Firstly, we consider $CH_3NH_3SnBr_3$ in the cubic phase. As it clearly comes out from panel I of Fig. 4, the cubic phase of $CH_3NH_3SnBr_3$ shows a direct gap E_g=1.04 eV at the R point.[28] This is a typical characteristic of $CH_3NH_3MX_3$ compounds.[29] The band structure of $CH_3NH_3SnCl_3$ in the monoclinic phase[30] is reported in Fig. 5. As shown in panel I of Fig. 5, the $CH_3NH_3SnCl_3$ compound is characterized by a direct gap at the B point with an energy gap E_g of 1.94 eV.

Due to the well known underestimation of transition energies within density functional theory, we applied GW corrections to the DFT-GGA energy gaps. The DFT-GGA band gaps as well as the GW corrected results are reported in the last two columns of Table II, in fair agreement with the experimental measurements.

Further insight can be obtained by analyzing the total density of states (DOS) and the projected density of states (PDOS) for both compounds. The projection is done onto the atomic orbitals of each atom. The DOS and PDOS of $CH_3NH_3SnBr_3$ and $CH_3NH_3SnCl_3$ are shown in Figs. 4 and 5, respectively, evidencing an overall similarity. The total DOS (in gray) as well as the projection on SnX_3 (in black) are shown in panel II of both figures. The visible part of the gray shadow is related to the $CH_3NH_3^+$ cation contribution to the total DOS and it is in correspondence (see panel I) to flat bands of the electronic band structure. No cation contribution

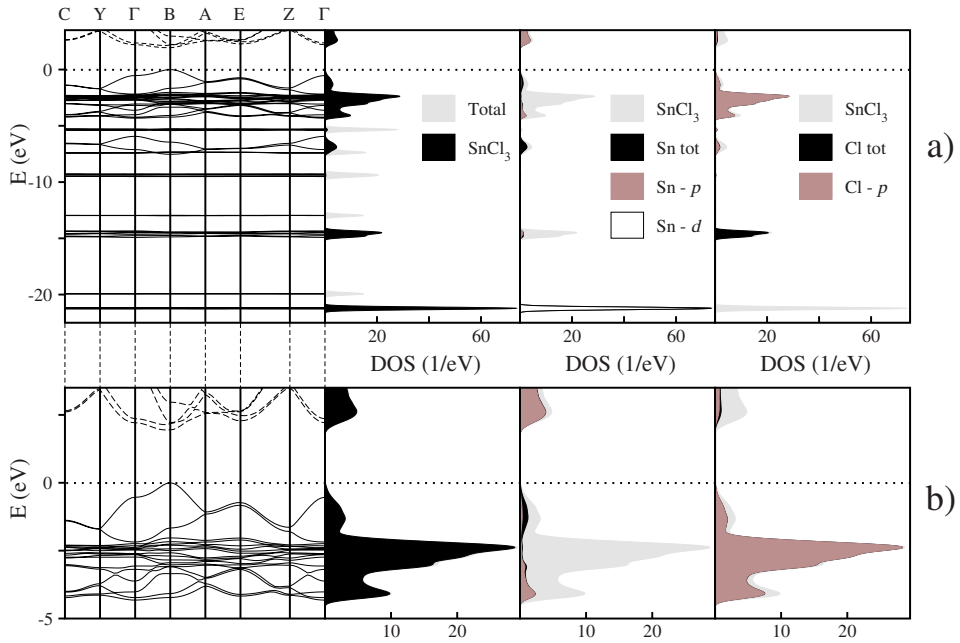

FIG. 5. (Color online) The calculated band structure and the total and the projected density of states for $CH_3NH_3SnCl_3$ in the monoclinic phase. In panel I, the band structure is shown along the high symmetry directions in the Brillouin zone. In panel II, the total DOS (gray) is represented along with the projection on $SnCl_3$ (black). The visible part of the gray shadow is related to the $CH_3NH_3^+$ cation, in correspondence to flat bands. In panels III and IV, the projected DOS on Sn and Cl, respectively, is shown. A closer view of the near band region is shown in (b). Solid (dashed) lines represent full (empty) bands. The dotted line indicates the top of the valence band, set to zero.

occurs in the near-band-gap region for both compounds, as it is evidenced in Figs. 4(b) and 5(b). In panel III, the contribution of the Sn atoms to the total DOS is shown, along with the total contribution of the atoms of the perovskitic cage (SnX_3). The Sn *s*, Sn *p*, and Sn *d* valence orbitals are considered. The black shadow represents the Sn DOS, while the Sn *p* and Sn *d* PDOSs are shown in brown and white, respectively. The Sn *s* contribution is represented by the visible part of the black shadow. Similarly, the contribution of the halogen (Br and Cl, respectively) is represented in panel IV of both figures. In the case of Br (Fig. 4) *s*, *p*, and *d* valence orbital contributions are considered (the *d* contribution is represented by the visible part of the black shadow), whereas, in the case of Cl (Fig. 5), the *s* and *p* valence orbitals are taken into account.

Some points should be highlighted here: (i) For both compounds, it is found that the valence bands are dominated by the *X* (Br,Cl) *p* orbital contribution, while the conduction band is essentially dominated by the Sn *p* states, with a minor admixture from Br *p* and Br *d* states for $CH_3NH_3SnBr_3$ and Cl *p* states for $CH_3NH_3SnCl_3$; (ii) a clear separation of the regions with mainly *s* or mainly *p* characters comes out (this holds for *s* and *p* states) of both Sn and the halogen atoms; (iii) the *p* states of Sn mostly lie above the zero of energy, supporting the conclusion of essential ionization of Sn atoms; (iv) there is a very slight superposition between the projections of the valence band DOS on the Sn and the halogen, as it is clearly demonstrated by a comparison of panels III and IV.

All these observations suggest that there is a negligible hybridization between Sn and the halogen, confirming the ionic character of these compounds.

V. CONCLUSIONS

In conclusion, thin films of $CH_3NH_3SnX_3$ compounds (with X=Br,Cl) have been grown and their structural, optical, and electronic properties characterized. Structural calculations on the $CH_3NH_3SnCl_3$ monoclinic phase and $CH_3NH_3SnBr_3$ cubic phase agree well with the measured lattice parameters, as determined from x-ray analysis. The comparison of the absorption measurements with the theoretical calculations allows us to assign the absorption onset for both compounds to a direct gap transition, with the relevant energy levels strongly associated with the inorganic cage. Both experimental and theoretical analysis indicates that in this type of structure, the band gap mainly depends on SnX_3 pseudocubic cage size and ionicity, while the $CH_3NH_3^+$ cation plays the role only of an electron donor in the system. Moreover, the particular choice of the cation may affect the size of the pseudocubic cell, so modifying the band-gap value. For example, experimental results obtained by Yamada *et al.*[23] on the cubic phase of $CsSnCl_3$ and $CH_3NH_3SnCl_3$ show that the substitution of the Cs^+ with $CH_3NH_3^+$ increases the lattice constant by about 3% (from 5.6 to 5.76 Å). By changing the cation, and, in particular, its size, it is possible to increase considerably the cubic cell size: Mitzi and Liang[31] showed that the cubic perovskite $NH_2CH{=}NH_2SnI_3$ has a lattice constant approximately 1.2% larger than that for the isostructural $CH_3NH_3SnI_3$ compound. Consequently, this can be seen as a way of tuning the band gap of these direct gap semiconductors.

ACKNOWLEDGMENTS

F.C. acknowledges the support of Regione Emilia Romagna-Progetto MISTER. The calculations were performed at CINECA-Bologna "Iniziativa Calcolo Parallelo del CNR-INFM."

[1] David B. Mitzi, in *Progress in Inorganic Chemistry*, edited by K. D. Karlin (Wiley, New York, 1999), Vol. 48.
[2] S. N. Ruddlesden and P. Popper, Acta Crystallogr. **10**, 538 (1957).
[3] D. B. Mitzi, K. Chondroudis and C. R. Kagan, IBM J. Res. Dev. **45**, N1 (2001).
[4] D. B. Mitzi, C. A. Fiedl, W. T. A. Harrison, and A. M. Guloy, Nature (London) **369**, 467 (1994).
[5] P. Zhou, J. E. Drumheller, B. Patyal, and R. D. Willett, Phys. Rev. B **45**, 12365 (1992).
[6] M. Era, S. Morimoto, T. Tsutsui, and S. Saito, Appl. Phys. Lett. **65**, 676 (1994).
[7] C. R. Kagan, D. B. Mitzi, and C. D. Dimitrakopoulos, Science **286**, 945 (1999).
[8] D. B. Mitzi, Chem. Mater. **13**, 3283 (2001).
[9] O. Knop, R. E. Wasylishen, M. A. White, T. S. Cameron, and M. J. M. van Oort, Can. J. Chem. **68**, 412 (1990); R. E. Wasylishen, O. Knop, and J. B. Macdonald, Solid State Commun. **56**, 581 (1985); Q. Xu, T. Educhi, H. Nakayama, N. Nakamura, M. Kishita, and Z. Naturforsch, Z. Naturforsch., A: Phys. Sci. **46a**, 240 (1991).
[10] K. Yamada, S. Nose, T. Umeraha, T. Okuda, and S. Ichiba, Bull. Chem. Soc. Jpn. **61**, 4265 (1988).
[11] N. Onoda-Yamamuro, O. Yamamuro, T. Matsuo, H. Suga, K. Oikawa, N. Tsuchiya, T. Kamiyama, and H. Asano, Physica B **213-214**, 411 (1995).
[12] D. B. Mitzi, C. A. Fiedl, Z. Schlesinger, and R. B. Laibowitz, J. Solid State Chem. **114**, 159 (1995).
[13] K. Yamada, H. Kawaguchi, T. Matsui, T. Okuda, and S. Ichiba, Bull. Chem. Soc. Jpn. **63**, 2521 (1990).
[14] F. Chiarella, P. Ferro, F. Licci, M. Barra, M. Biasiucci, A. Cassinese, and R. Vaglio, Appl. Phys. A: Mater. Sci. Process. **86**, 89 (2007).
[15] S. Baroni, A. Dal Corso, S. de Gironcoli, P. Giannozzi, C. Cavazzoni, G. Ballabio, S. Scandolo, G. Chiarotti, P. Focher, A. Pasquarello, K. Laasonen, A. Trave, R. Car, N. Marzari, and A. Kokalj, http://www.quantum-espresso.org
[16] D. Vanderbilt, Phys. Rev. B **41**, 7892 (1990).

[17] N. Troullier and J. L. Martins, Phys. Rev. B **43**, 1993 (1991).
[18] J. P. Perdew, J. A. Chevary, S. H. Vosko, K. A. Jackson, M. R. Pederson, D. J. Singh, and C. Fiolhais, Phys. Rev. B **46**, 6671 (1992).
[19] H. J. Monkhorst and J. D. Pack, Phys. Rev. B **13**, 5188 (1976).
[20] G. Onida, L. Reining, and A. Rubio, Rev. Mod. Phys. **74**, 601 (2002).
[21] X. Gonze *et al.*, Z. Kristallogr. **220**, 558 (2005); http://www.abinit.org
[22] J. P. Perdew, K. Burke, and M. Ernzerhof, Phys. Rev. Lett. **77**, 3865 (1996).
[23] K. Yamada, Y. Kuranaga, K. Ueda, S. Goto, T. Okuda, and Y. Furukawa, Bull. Chem. Soc. Jpn. **71**, 127 (1998).
[24] C. Kittel, *Introduction to Solid State Physics*, 5th ed. (Wiley, New York, 1976).
[25] J. I. Pankove, *Optical Processes in Semiconductors* (Prentice-Hall, Englewood, NJ, 1971).
[26] H. Ishida, H. Maeda, A. Hirano, Y. Kubozono, and Y. Furukawa, Phys. Status Solidi A **159**, 277 (1997).
[27] A. Maalej, Y. Abid, A. Kallel, A. Daoud, A. Lautie, and F. Romain, Solid State Commun. **103**, 279 (1997).
[28] The dispersion curves are shown along the directions $\Gamma \rightarrow R \rightarrow \Gamma \rightarrow X \rightarrow M \rightarrow \Gamma \rightarrow X$, where $\Gamma \equiv (0,0,0)$, $R \equiv (\frac{1}{2},\frac{1}{2},\frac{1}{2})$, $X \equiv (0,\frac{1}{2},0)$, and $M \equiv (\frac{1}{2},\frac{1}{2},0)$.
[29] I. B. Koutselas, L. Ducasse, and G. C. Papavassiliou, J. Phys.: Condens. Matter **8**, 1217 (1996).
[30] The dispersion curves are shown along the directions $C \rightarrow Y \rightarrow \Gamma \rightarrow B \rightarrow A \rightarrow E \rightarrow Z \rightarrow \Gamma$, where $C \equiv (0,\frac{1}{2},\frac{1}{2})$, $Y \equiv (0,\frac{1}{2},0)$, $\Gamma \equiv (0,0,0)$, $B \equiv (-\frac{1}{2},0,0)$, $A(-\frac{1}{2},-\frac{1}{2},0)$, $E \equiv (-\frac{1}{2},-\frac{1}{2},\frac{1}{2})$, and $Z(0,0,\frac{1}{2})$.
[31] D. B. Mitzi and K. Liang, J. Solid State Chem. **134**, 376 (1997).